Turbulent Inflow Generation by Resolvent Mode Forcing

Björn Selent[1(✉)], Christoph Wenzel[1], Ulrich Rist[1], and Oliver T. Schmidt[2]

[1] University of Stuttgart, Institute of Aerodynamics and Gas Dynamics, 70550 Stuttgart, Germany
selent@iag.uni-stuttgart.de
[2] Department of Mechanical and Aerospace Engineering, University of California San Diego, La Jolla, CA 92093-0411, USA

Abstract. The present article deals with turbulent inflow generation for use in large eddy or direct numerical simulations of boundary layer flows. The turbulent inflow is generated by synthetic volume forcing. The spatial and temporal properties of the synthetic eddies are obtained from resolvent mode analysis of turbulent mean data of a flat-plate flow at a Reynolds number range $\mathrm{Re}_\theta = 300 - 1100$ and inserted into the same mean flow in subsequent direct numerical simulations. Both integral as well as local turbulent mean-statistics of the resulting unsteady flow field show very good agreement compared to results of high fidelity simulations of the same flow regime. The recovery length is comparable to classical methods while suppressing unphysical noise at the inflow. Additionally, the results hint at a Reynolds number independency of the proposed approach.

Keywords: Turbulent inflow generation · Numerical simulations · Synthetic volume forcing · Resolvent mode analysis

1 Introduction

The accurate numerical representation of turbulent wall-bounded flow still is an area of high scientific and engineering interest because of its relevance in most technical applications. In the case of high fidelity numerical simulations the matter arises of how a statistically fully developed turbulent flow is obtained as fast and with as little computational effort as possible. Additionally it is beneficial if the method is computationally robust, local, i.e. does not need parallelization, and allows to be generalized.

Three main approaches have been established in the last quarter century, namely the simulation of all transition stages from laminar to turbulent flow, temporal or spatial reuse of precomputed solutions at an upstream station of the flow (recycling and rescaling methods, RRM) and the introduction of artificial turbulent flow structures along the boundaries (synthetic turbulence generators, STG). Simulations of the full transition process start off from a laminar base

A. Dillmann et al. (Eds.): DGLR 2018, NNFM 142, pp. 110–119, 2020.
https://doi.org/10.1007/978-3-030-25253-3_11

and trigger the transition by exciting harmonic or pulsed perturbations which undergo amplification and nonlinear interaction processes leading to turbulent flow. Usually this approach uses the longest domain in order to obtain fully established turbulent statistics at a desired Reynolds number position and has been applied e.g. by Schlatter et al. [9] for instance. Methods known as strong recycling reuse unsteady results of turbulent flow. These data can be obtained simultaneously as e.g. in Spalart [12] or from preceding auxiliary computations. In order to overcome so-called box-periodicity and to reduce the computational effort, Wu et al. [18] developed a weak recycling method which rescales the re-introduced velocity field according to boundary layer parameters. Thus it is possible to use downstream results as inflow condition in non-homogeneous directions. RRM allow for a start of simulations at locations close to the domain of interest and is thus well suited for LES or DNS of engineering flows at moderately large Reynolds numbers (see Lund et al. [5] or Pirozzoli [7] for example). Wu [17] reported the amplification of small acoustic disturbances especially in the freestream for RRM though.

The third approach (STG) comprises all methods which generate synthetic turbulence. Béchara et al. [1] composed the turbulent velocities from random Fourier modes which they fitted to a given turbulent energy spectrum. Temporal correlation was ensured via filtering. Klein et al. [4] transferred the idea of digital filtering to generate a spatially correlated turbulent flow field from random numbers whereas Jarrin et al. [2] modeled characteristic flow features such as streaks and vortices rather than the underlying spectra. Schemes which ensure spatial properties are often summarized as Synthetic Eddy Methods (SEM). Recent work of Rout [8] used modal perturbations computed from resolvent analysis (RA) which he superposed to match near-wall streaks and hairpin vortices. Spille-Kohoff and Kaltenbach [13] use additional volume forcing terms of the Navier-Stokes-equations to excite fluctuations in the flow in a further branch of synthetic methods. Keating et al. [3] compared STG to RRM and concluded that RRM leads to faster transition. Depending on the actual implementation both STG and RRM are computationally demanding especially when filter or scaling operations need data to be exchanged between subprocesses. Furthermore the use of random data in many synthetic generators may lead to noise pollution which impedes its use in computational aero-acoustic simulations (CAA). The aforementioned methods are by no means exhaustive and variations, adaptations and optimizations to particular flow configurations exist.

The reader is referred to the comprehensive review of Wu [17]. The common denominator of RRM and STG is the need for a realistic spectral content of the turbulent flow field to rapidly reach a fully developed turbulent state. Methods that start off from turbulent state generally match the inflow to known first and second order statistics. The data is drawn from semi-empirical energy and velocity distributions or actual flow data from preceding numerical simulations and experiments. This inherently limits the general applicability of those methods somewhat, especially if flows with pressure gradients are investigated for which these data are generally unknown. In case of laminar-turbulent transition,

the perturbations are obtained from eigenvalue analysis of the initially steady base-flow. This makes the approach widely applicable at the expense of a necessarily larger computational domain. Rout's work picks up the idea to solemnly use first order statistics, i.e. mean flow data, to compute the input fluctuations from.

Objectives. We present a combination of volume forcing with Rout's ansatz to gain input perturbations for turbulent boundary layer (TBL) flow simulations. The volume forces are obtained from superposition of two-dimensional forcing modes computed over a range of frequencies and spanwise wavenumbers. These modes are solutions to an optimization problem of the resolvent operator introduced by Trefethen et al. [14]. The generated forces exploit optimal transient growth to stir the mean-flow into a fully developed turbulent state. The resolvent mode forcing method (RFM) presented in this work thus offers an alternative approach for generating realistic turbulent inflow fields for DNS and LES computations. Its largest benefit is the sole dependence on mean-flow parameters to compute the unsteady input terms. This not only obliterates the need of higher-order reference data but allows for simulations beginning at larger Reynolds numbers where the matching of the statistics becomes more difficult due to the multi-layer character of the TBL. Furthermore RFM is an algorithmically simple method due to its formulation as local source term. The need for computationally expansive trigonometric functions can be reduced to a small subset of grid nodes. Finally the erroneous noise introduced by the excitation is minimized thus making the method suitable for aero-acoustic simulations as well.

2 Numerical Method

Direct Numerical Simulations. The direct numerical simulations have been done using the inhouse code *ns3d* [15]. It solves the fully unsteady three-dimensional compressible Navier-Stokes equations in conservative formulation on structured meshes. The governing equations are

$$\frac{\partial \rho}{\partial t} = -\nabla \cdot \rho \mathbf{u}, \tag{1a}$$

$$\frac{\partial \rho \mathbf{u}}{\partial t} = -\nabla \cdot (\rho \mathbf{u} \otimes \mathbf{u}) - \nabla p + \nabla \cdot \tau + \rho \mathbf{f}, \tag{1b}$$

$$\frac{\partial e}{\partial t} = -\nabla \cdot [(e+p)\mathbf{u}] + \frac{1}{(\kappa-1)\mathrm{Re}\,\mathrm{Pr}\,\mathrm{Ma}_\infty^2} \nabla \cdot (\mu \nabla T) + \nabla \cdot (\tau \mathbf{u}), \tag{1c}$$

where ρ is the density, $\mathbf{u} = (u, v, w)^T$ the vector of Cartesian velocity components in x, y and z direction resp., p pressure, $\mathbf{f}$ volume forces, e total energy, T temperature and t time. The dynamic viscosity μ is a fluid property and $\tau = \frac{\mu}{\mathrm{Re}} \left[\left(\nabla \mathbf{u} + \nabla \mathbf{u}^T \right) - \frac{2}{3} (\nabla \cdot \mathbf{u}) \mathsf{I} \right]$ the viscous stress tensor (I being the identity matrix). All quantities are non-dimensionalized either by their respective free-stream values $(.)^*_\infty$ or the boundary-layer thickness at the inflow δ_0. The dimensionless time is $t = t^* \frac{\delta_0}{u^*_\infty}$. Hence the flow is fully described by providing Reynolds number $\mathrm{Re} = \rho^*_\infty u^*_\infty \delta_0 / \mu^*_\infty$, Prandtl number $\mathrm{Pr} = c^*_\mathrm{p} \mu^*_\infty / k^*_\infty$,

and Mach number $\mathrm{Ma} = u^*_\infty / a^*_\infty$. The set of governing Eq. (1) is closed by the equation of state for an ideal gas $p = \rho T/(\kappa \mathrm{Ma}^2_\infty)$ and Sutherland's law $\mu(T) = T^{3/2}(1+T_s)/(T+T_s)$ with the Sutherland temperature $T_s = 110.4\,\mathrm{K}/T^*_\infty$. Spatial derivatives are approximated with alternating finite differences of eighth order and time is integrated by a classical fourth-order four-stage Runge-Kutta scheme. Unless mentioned otherwise, characteristic conditions for subsonic flow are applied at the inflow and freestream domain boundaries, the lower boundary consists of an adiabatic no-slip wall and at the outflow the time derivative of the solution vector is extruded from the interior $\frac{\partial \mathbf{q}}{\partial t}|_n = \frac{\partial \mathbf{q}}{\partial t}|_{n-1}$. Towards the outflow and freestream boundaries the grid is stretched and the solution is filtered to minimize perturbations reflecting from the boundaries.

Resolvent Analysis. The spatial and temporal structure of the forcing functions in (1)

$$\mathbf{f}(x,y,z,t) = \hat{\mathbf{f}}(x,y)\mathrm{e}^{\mathrm{i}(\gamma z - \omega t)} \tag{2}$$

are taken to be harmonic in spanwise direction and time with wavenumbers γ and frequencies ω. They are obtained from resolvent analysis of the mean state of the flow in a streamwise wall-normal plane. The algorithm is outlined in detail in Schmidt et al. [10]. The basic idea is to find a forcing to the linear equations

$$(-\mathrm{i}\omega \mathsf{I} - \mathsf{L})\,\hat{\mathbf{q}} = \mathsf{B}\hat{\mathbf{f}} \tag{3}$$

such that the response $\hat{\mathbf{q}} = [\hat{\rho}, \hat{\mathbf{u}}, \hat{T}]^{\mathrm{T}}(x,y)\mathrm{e}^{\mathrm{i}(\gamma z - \omega t)}$ is maximized. L is the operator resulting from a linearization of (1) and the sponge matrix B is used to restrict the forcing to a disturbance strip of width $\Delta x = 1$ (cf. Fig. 1). A measure for the optimality of the forcing is the norm of the resolvent operator $\mathsf{R} = (-\mathrm{i}\omega \mathsf{I} - \mathsf{L})^{-1}\mathsf{B}$

$$\|\mathsf{R}\| \equiv \sup_{\hat{\mathbf{f}}} \frac{\|\hat{\mathbf{q}}\|}{\|\hat{\mathbf{f}}\|} \tag{4}$$

which quantifies the rate of amplification or gain in the process. Equations (3) and (4) constitute an optimization problem for $\hat{\mathbf{f}}$ which can be solved by a singular value decomposition (SVD) of the weighted resolvent operator

$$\tilde{\mathsf{R}} = \mathsf{W}_{\mathbf{q}}^{1/2}\mathsf{R}\mathsf{W}_{\mathbf{f}}^{-(1/2)} = \tilde{\mathsf{Q}}\tilde{\Sigma}\tilde{\mathsf{F}}^H. \tag{5}$$

The input weights $\mathsf{W}_{\mathbf{q}}$ and output weights $\mathsf{W}_{\mathbf{f}}$ ensure orthonormality of the singular vectors of the response $\tilde{\mathbf{q}}$ and forcing $\tilde{\mathbf{f}}$ respectively. $\Sigma = \mathrm{diag}(\sigma_1, \sigma_2, \ldots, \sigma_N)$ contains the amplitude gains. The SVD is done by first discretizing Eq. (3) by fourth-order summation by parts finite differences from Mattsson et al. [6] and solving the eigenvalue problem

$$\mathsf{W}_{\mathbf{f}}^{-1}\tilde{\mathsf{R}}^H\mathsf{W}_{\mathbf{q}}\tilde{\mathsf{R}}\hat{\mathbf{f}} = \sigma^2\hat{\mathbf{f}} \tag{6}$$

for the largest eigenvalues with a standard Arnoldi method.

3 Results

Simulations have been performed for the setup reported in Wenzel et al. [16] which employed a digital-filtering SEM [4] to generate the inflow perturbations. The initial condition consists of the statistically converged two dimensional turbulent mean flow $\mathbf{Q} = [\bar{\rho}, \tilde{\mathbf{u}}, \bar{T}]^{\mathrm{T}}$ from [16], where $\bar{(\cdot)}$ indicates the Reynolds average. A two dimensional cut serves as baseflow to the resolvent mode computations where grid points are clustered inside the boundary layer and at the position of the forcing zone. Further simulations have been performed to assess the RFM's potential to start at positions farther downstream. Therefore, a new set of resolvent modes has been computed within a domain shifted downstream by $\Delta \mathrm{Re}_\theta = 370$. The setup of the DNS has been kept except for a cut of the domain length at $x_{\mathrm{Re}_\theta=670}$. An overview of the simulation parameters is listed in Table 1. A schematic overview of the computational domain for both the DNS and RA is shown in Fig. 1.

Table 1. Physical and computational parameters of the numerical simulations

$\mathrm{Re} = 3000$, $\mathrm{Ma} = 0.85$, $\mathrm{Pr} = 0.71$			
	$\mathrm{Re}_{\theta,0}$	$l_x \times l_y \times l_z$	$n_x \times n_y \times n_z$
RA, 300	300	$100\delta_0 \times 4.4\delta_0 \times 0$	$555 \times 95 \times 1$
SEM/RFM, 300	300	$400\delta_0 \times 96\delta_0 \times 4\pi\delta_0$	$1560 \times 240 \times 256$
RA, 670	670	$100\delta_0 \times 4.4\delta_0 \times 0$	$555 \times 95 \times 1$
RFM, 670	670	$345\delta_0 \times 96\delta_0 \times 4\pi\delta_0$	$1200 \times 240 \times 256$

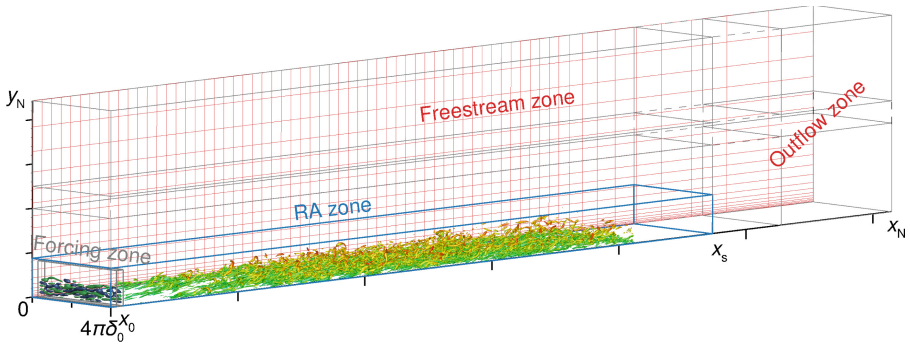

Fig. 1. Computational domain: towards the outflow and freestream boundaries the grid is stretched. The blue box outlines the domain used in the modal analysis. The forcing ist introduced in the small box close to the inflow boundary.

Resolvent Mode Computation. The resolvent modes, i.e. the gains and eigenfunctions of the forcing have been computed for equidistantly spaced ranges of

dimensionless frequency $\mathrm{St} \in [0.01, 1]$ with step size $\Delta\mathrm{St} = 0.033$ and wavenumber $\gamma \in [0, 15]$ with $\Delta\gamma = 0.5$. For each St and γ the five leading modes have been computed. The spectrum of the modes is shown in Fig. 2. The largest gain for each St-γ combination can be seen in the low frequency, low wavenumber portion of the spectrum. The modal structures are of the size of δ and may be interpreted as large-scale eddies that stir the mean flow to generate turbulent fluctuations. From this set of solutions 113 modes with $\sigma \geq 15$ are used as input for the DNS. The threshold value has been increased to $\sigma \geq 20$ to reach a similar quantity of modes for the shifted DNS. The amplitudes of the eigenfunctions $\hat{\mathbf{f}} = [\hat{\mathbf{u}}, \hat{\mathbf{v}}, \hat{\mathbf{w}}]^{\mathrm{T}}$ are eventually scaled by the maximum of the amplitudes $\sup \|\hat{f}_i\|$.

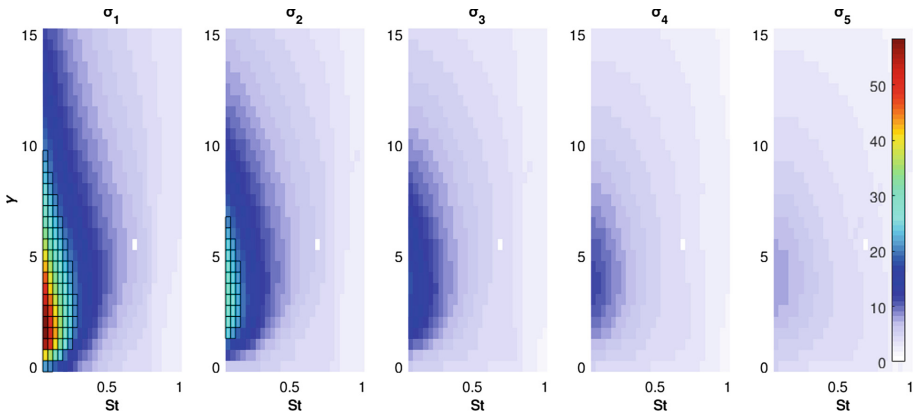

Fig. 2. Gains distribution of dominant (σ_1) and four sub-dominant resolvent modes (σ_{2-5}) versus Strouhal number and spanwise wave number. Framed Modes have $\sigma \geq 15$ and are used for the DNS.

Direct Numerical Simulation. The main simulation has been run for 240 000 time steps with $dt = 0.0335$. This corresponds to four flow-through times and ensures that any transients left the computational domain. The flow field at every 10th of 120 000 time steps altogether has been sampled and the temporal and spanwise mean- and root-mean-square values have been computed. This data then has been used to compute local and integral measures of the flow.

The method's proficiency is first evaluated by comparing the wall-friction coefficient c_f and integral parameters of the resulting TBL to the data from Wenzel et al. [16]. In Fig. 3**a** the c_f of the RFM simulation follows the SEM curve but overshoots within an initial length of $50\delta_0$. Afterwards the lines collapse and follow the theoretical gradient. The shape factor $H = \delta^*/\theta$ shown in Fig. 3**b** also follows the trend of the SEM but does show a steeper gradient and recovers the validated value of $H \approx 1.8$ after $50\delta_0$. From Fig. 3**b** it can be seen that the boundary-layer thickness computed from the RFM is larger by a maximum value of 3% for about half the domain length but follows the SEM trend. Similarly the displacement thickness δ^* and the momentum thickness θ align with their

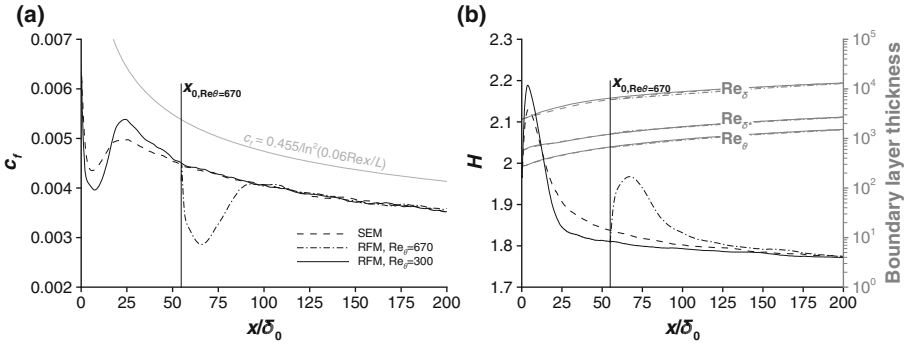

Fig. 3. Comparison of turbulent boundary layer parameters. **a** Friction coefficient. **b** Shape factor and boundary-layer thickness.

SEM counterparts. The displacement thickness even depicts the same bump at the very origin which correlates to the maximum in H at $x = 3.7$.

The temporal and spanwise mean values of the downstream velocity component U^+_{VD} have been computed for $\mathrm{Re}_\theta = 670$, 1000 and 1410 and scaled by *van-Driest*'s transformation. This allows for the additional comparison with an incompressible reference from Schlatter et al. [9]. Results are plotted with inner scaling in Fig. 4**a**. For $\mathrm{Re}_\theta = 670$ the velocity defect $u_\infty - \bar{u}$ of the RFM solution is too large in the wake and potential region but with increasing Re_θ this excess defect decreases and fits with both the SEM and the incompressible reference. The viscous sublayer ($y^+ \lesssim 10$), the buffer ($10 < y^+ \lesssim 50$) and the overlap region ($50 < y^+ \lesssim 300$) show good agreement for all considered Re_θ. The turbulent intensities are plotted in Fig. 4**b**. The Morkovin-scaled rms-values of the velocity components are normalized with the wall friction velocity u_τ and show good agreement with the references. The u^+_{M} and w^+_{M} values are underestimated in the overlap and wake region ($0.3 \lesssim y/\delta \lesssim 0.8$) for $\mathrm{Re}_\theta = 670$ and $\mathrm{Re}_\theta = 1000$. For $\mathrm{Re}_\theta = 1410$ the solutions match the references throughout the boundary layer. The wall-normal fluctuations v^+_{M} are already in better agreement at the upstream station hinting that the wall-normal velocity is the least sensitive to the inputs.

The RFM introduces forcing terms to the momentum equations only, thus the thermodynamic quantities T, ρ and p are only affected indirectly through the coupling of the energy equation and mass conservation. To assess the adequacy of this approach the fluctuations of the temperature $T'^+ = \sqrt{\bar{T'^2}}/(\kappa \mathrm{Ma}^2 u_\tau^2)$ and pressure $p^+ = \sqrt{\bar{p'^2}}/(\rho_W u_\tau^2)$ have also been computed and are shown in Figs. 5**a** and **b** respectively. The temperature's curvature is less pronounced in the regions above the viscous sublayer at the early stages. With increasing Reynolds number the gradients converge to the SEM solution. The pressure fluctuations' slope, too, is almost constant in the wake region at $\mathrm{Re}_\theta = 670$. Unlike the SEM solution the RFM does not exhibit the large overshoot within the viscous regions though.

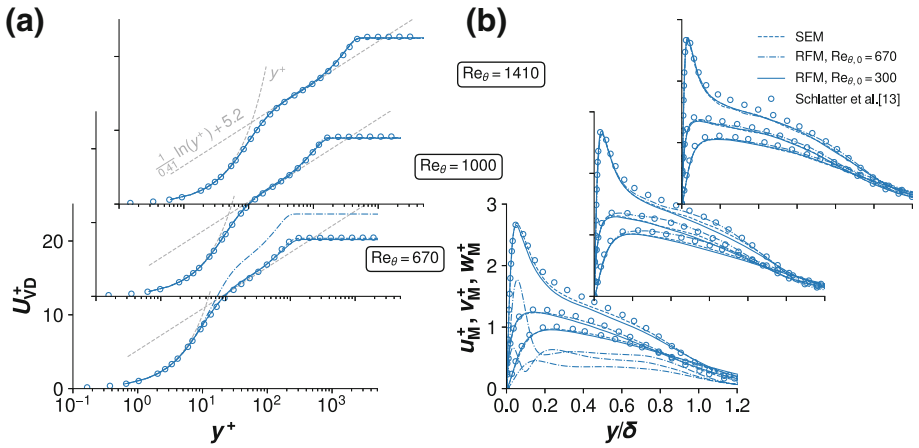

Fig. 4. Comparison of local velocities of turbulent boundary layer. **(a)** van-Driest transformed mean-velocity profile. **(b)** Morkovin scaled turbulent intensities.

Perturbations in the SEM are introduced as primitive variables at the inflow and thus generate a noise source at the wall. The SEM's pressure overshoot prevails until $\mathrm{Re}_\theta = 1410$ as does the constant slope of the RFM pressure fluctuations. From $\mathrm{Re}_\theta = 1410$ the RFM solution follows the reference's curvature with the maximum amplitude being ≈0.5% smaller.

Figures 3, 4 and 5 also include results for the second DNS. Here the friction coefficient establishes after a slightly shorter length $\Delta\delta|_{c_f,\mathrm{Re}_\theta=670}/\Delta\delta|_{c_f,\mathrm{Re}_\theta=300} = 70\%$ compared to the initial setup. The shape factor takes longer on the other hand with $\Delta\delta|_{H,\mathrm{Re}_\theta=670}/\Delta\delta|_{H,\mathrm{Re}_\theta=300} = 130\%$. The mean velocity profiles at $\mathrm{Re}_\theta = 670$ show an offset in the wake due to the falsely estimated friction coefficient. Besides this offset the mean flow is upheld as expected. At $\mathrm{Re}_\theta = 1000$ the mean velocity is en par with the previous simulations. The u_M^+-values, too, have almost fully recovered and match the curvature and amplitudes of Schlatter et al.'s [9] solution. The transversal velocities v_M^+ and w_M^+ are too large in amplitude in the overlap and wake region, though. The reason for that is not yet clear. At $\mathrm{Re}_\theta = 1410$ the results collapse with the results of all compressible computations except for the wake where a small excess prevails. The temperature and pressure fluctuations at $\mathrm{Re}_\theta = 670$ are too low in amplitude and are constant for parts of the overlap and wake region. Temperature and turbulent intensities are not in equilibrium at the forcing station yet because no measures have been taken to ensure a consistent state, i.e. a constant turbulent Prandtl number $\mathrm{Pr}_t = \frac{\overline{u'v'}}{\overline{v'h'}} \frac{\partial \tilde{T}/\partial y}{\partial \tilde{u}/\partial y} \approx 1$. Judging from Fig. 5 the temperature and pressure fluctuations have nonetheless already reached a realistic distribution at $\mathrm{Re}_\theta = 1000$. Both temperature and pressure still show an amplitude overshoot but follow the gradient of the references. At $\mathrm{Re}_\theta = 1410$ the curves show good agreement except for a an overestimated amplitude in the wake of the temperature profile. Both temperature and pressure fluctuations vanish in the freestream.

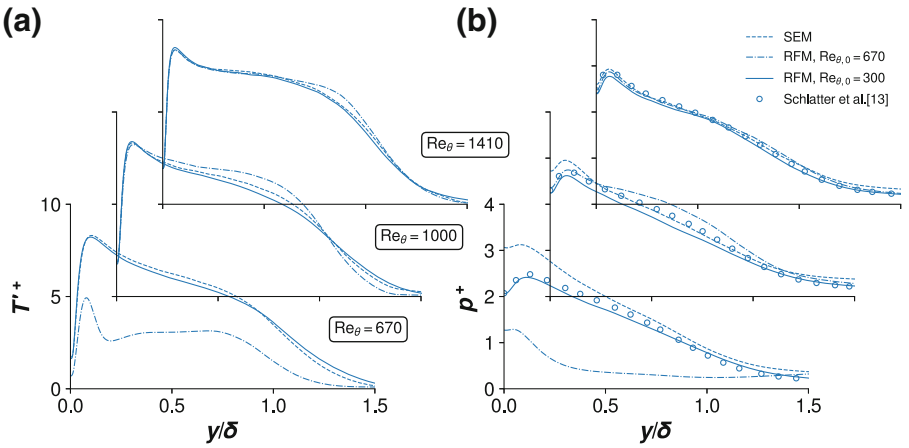

Fig. 5. Comparison of local thermodynamic parameters of turbulent boundary layer. **(a)** Static temperature fluctuations. **(b)** Pressure fluctuations.

4 Conclusions

We have presented an alternative method to generate fully turbulent flow in DNS or LES simulations of compressible boundary-layer flows with the help of suitable perturbation functions obtained from resolvent analysis. The mode, i.e. the perturbation computation relies on the mean values of the considered flow configuration only. Direct numerical simulations that have been done so far show promising results and demonstrate the general suitability of the approach. The novel method is comparatively easy to implement in existing DNS solvers. Simulations with the RFM yield both realistic turbulent velocity fields and thermodynamic parameters. The shape factor and the skin friction can be recovered at induction lengths comparable to established methods such as SEM but is still larger than more recently optimized schemes (e.g. Shur et al. [11]). The formulation as a source to the momentum equations avoids erroneous pressure disturbances at the inflow which makes the RFM a candidate to CAA simulations, too. A first test has confirmed that the RFM is not sensitive to the chosen inflow Reynolds number. It is not yet fully understood how the solution depends on the set of resolvent modes used as perturbation functions. This certainly remains to be further looked into.

References

1. Béchara, W., Bailly, C., Lafont, P.: Stochastic approach to noise modelling for free turbulent flows. AIAA J. **32**(3), 455–463 (1994)
2. Jarrin, N., Benhamadouche, S., Laurence, D., Prosser, R.: A synthetic-eddy-method for generating inflow conditions for large-eddy simulations. Int. J. Heat Fluid Flow **27**(4), 585–593 (2006). Special Issue of The Fourth International Symposium on Turbulence and Shear Flow Phenomena - 2005
3. Keating, A., Piomelli, U., Balaras, E., Kaltenbach, H.J.: A priori and a posteriori tests of inflow conditions for large-eddy simulation. Phys. Fluids **16**, 4696–4712 (2004)
4. Klein, M., Sadiki, A., Janicka, J.: A digital filter based generation of inflow data for spatially developing direct numerical or large eddy simulations. J. Comput. Phys. **186**(2), 652–665 (2003)
5. Lund, T.S., Wu, X., Squires, K.D.: Generation of turbulent inflow data for spatially-developing boundary layer simulations. J. Comput. Phys. **140**, 233–258 (1998)
6. Mattsson, K., Nordström, J.: Summation by parts operators for finite difference approximations of second derivatives. J. Comput. Phys. **199**, 503–540 (2004)
7. Pirozzoli, S., Bernardini, M.: Turbulence in supersonic boundary layers at moderate reynolds number. J. Fluid Mech. **688**, 120–168 (2011)
8. Rout, V.: Analysis of resolvent method for turbulence inflow generation. Master's thesis, University of Melbourne (2018)
9. Schlatter, P., Li, Q., Brethouwer, G., Johansson, A.V., Henningson, D.S.: Simulations of spatially evolving turbulent boundary layers up to Re_θ=4300. Int. J. Heat Fluid Flow **31**(3), 251–261 (2010)
10. Schmidt, O.T., Towne, A., Rigas, G., Colonius, T., Brès, G.A.: Spectral analysis of jet turbulence. J. Fluid Mech. **855**, 953–982 (2018)
11. Shur, M., Spalart, P., Strelets, M., Travin, A.: Synthetic turbulence generators for RANS-LES interfaces in zonal simulations of aerodynamic and aeroacoustic problems flow. Turb. Comb. **93**, 63–92 (2014)
12. Spalart, P.R.: Direct simulation of a turbulent boundary layer up to $R_\theta = 1410$. J. Fluid Mech. **187**, 61–98 (1988)
13. Spille-Kohoff, A., Kaltenbach, H.J.: Generation of turbulent inflow data with a prescribed shear-stress profile. In: Liu, C., Sakell, L., Beutner, T. (eds.) DNS/LES Progress and Challenges, pp. 319–326. Greyden Press, Columbus (2001)
14. Trefethen, L.N., Trefethen, A.E., Reddy, S.C., Driscoll, T.A.: Hydrodynamic stability without eigenvalues. Phys. Fluids **15**(9), 2525–2540 (2003)
15. Wenzel, C., Peter, J.M.F., Selent, B., Weinschenk, M., Rist, U., Kloker, M.: DNS of compressible turbulent boundary layers with adverse pressure gradients. In: Nagel, W.E., Kröner, D., Resch, M. (eds.) High Performance Computing in Science and Engineering 2018. Springer, Cham (2018)
16. Wenzel, C., Selent, B., Kloker, M., Rist, U.: DNS of compressible turbulent boundary layers and assessment of data/scaling-law quality. JFM **842**, 428–468 (2018)
17. Wu, X.: Inflow turbulence generation methods. Ann. Rev. Fluid Mech. **49**, 23–49 (2017)
18. Wu, X., Squires, K.D., Lund, T.S.: Large eddy simulation of a spatially-developing boundary layer. In: Proceedings of the 1995 ACM/IEEE Conference on Supercomputing, Supercomputing 1995. ACM, New York (1995)